ORIGINAL PAPER

# Research on the Mechanical Properties of 3D Printing Polymer Reinforced Cemented Tailings Backfill Under Uniaxial Compression

**Zhiqiang Huang · Shuai Cao · Shiwen Qin**

**Abstract** The brittle damage of the cemented tailings backfill (CTB) seriously threatens the safety of underground workers and equipment. To improve the toughness and ductility characteristics of the CTB, a 3D printing polymer reinforced CTB was designed and prepared. In this study, the uniaxial compression and scanning electron microscopy tests were conducted to investigate the uniaxial compression strength (UCS), stress–strain curve, toughness index, failure mode, and hydration products. The results show that: the UCS of the 3D printing polymer reinforced CTB was 0.80 MPa, and the average UCS growth rate was 36.6% when the material type and shape were ordinary resin (OR) and cross-section. The toughness index (K) value of the 3D printing polymer reinforced CTB with the OR material type was more significant than that of the ordinary CTB. The main hydration products were ettringite and C–S–H gel. 3D printing polymer showed good toughness to the CTB. The research conclusions can provide an essential reference basis for industrial applications of underground backfill.

## 1 Introduction

Backfilling is a robust mining method for ground pressure management and ensuring underground mining safety. Cemented tailings backfill (CTB) or cemented paste backfill (CPB) technology has been widely used to fill underground goaf (Cao et al. 2020; Li et al. 2021; Huang et al. 2021a). This technology optimizes mining methods and significantly reduces the impact of toxic and hazardous substances in tailings on the groundwater environment (Liu et al. 2020a, b; 2021). A great deal of helpful exploration has been carried out by scholars at home and abroad about CTB and CPB. The main content covers uniaxial compressive strength, triaxial compressive strength, Hopkinson rod impact test, Brazilian split, three-point flexural strength, and shear strength (Min et al. 2019; Cheng et al. 2019; Hou et al. 2021; Xu et al. 2021; Zheng et al. 2021; Zhao et al. 2021; He et al. 2021). Numerous studies have shown that CTB exhibits significant brittleness during loading. The CTB loses strength instantaneously and fractures after loading to the peak. From an engineering point of view, the collapse and instability of CTB, whether in the cut and fill mining method or the open stope subsequent backfilling method, both can cause depletion of the ore and pose a serious threat to the

Z. Huang · S. Cao (✉) · S. Qin
School of Civil and Resource Engineering, University of Science and Technology Beijing, Beijing 100083, China
e-mail: sandy_cao@ustb.edu.cn

Z. Huang · S. Cao · S. Qin
Key Laboratory of High-Efficient Mining and Safety of Metal Mines, Ministry of Education, Beijing 100083, China

safety of underground operators and equipment (Zheng et al. 2020a, b; Wang et al. 2021b; Ding et al. 2021).

A great deal of research work has been carried out by domestic and international scholars and technicians on the brittle characteristics of the CTB. Xue et al. (2020; 2021) found that incorporating polypropylene fiber into the CTB can effectively improve its uniaxial compressive strength and flexural strength; Huang et al. (2021b) investigated three-point flexural tests with glass and polypropylene fiber incorporated into the CTB. Moreover, they found that the above two kinds of fiber can effectively improve its deflection; Xu et al. (2019) and Cao et al. (2019) concluded that the incorporation of fiber within the CTB can effectively slow down the crack expansion and restrain the deformation of the CTB. Wang et al. (2021a) found that incorporating rubber in the CTB could make it have higher ductility and toughness. Hamdaoui et al. (2021) found that the incorporation of Posidonia-Oceanica natural fiber substantially improved the ductility of CTB. Wang et al. (2020) concluded that the incorporation of straw fiber also increased the compressive strength of the CTB by up to 14.7%. Similarly, Chen et al. (2020) found that rice straw enhances the ductility of the CTB and maintains the integrity of the CTB in the event of damage.

Studies have shown that adding additive materials such as fiber, rubber, and straw to the CTB can effectively improve its toughness and ductility. Furthermore, the above research methods mainly focus on indoor uniaxial compression, three-point bending. However, it should not be overlooked that the rheological properties of the CTB slurry also change significantly when other additive materials are incorporated. It is prone to technical problems in engineering, such as blocked pipes and maintenance difficulties. Based on this, this paper will design and prepare a 3D-PP reinforced CTB from the indoor experiment. Furthermore, its macroscopic and microscopic properties were studied by uniaxial compression, failure evolution, and scanning electron microscopy. It is hoped that this will provide a theoretical basis for mine filling in the future.

## 2 Materials and Methods

### 2.1 Tailings, Cementitious Materials, and Water

The tailings in this experiment came from a gold mine in Shandong. Before the experiment, the gold tailings were dried in a thermostatic oven of model DGG-9240 for 12 h at 100 °C. The dried tailings were kept sealed to prevent rewetting in contact with air. Tianjin Fuyuan Ordinary Portland Cement 42.5R (OPC 42.5R) was used as the cementitious material for this experiment. The particle size distribution of the tailings and OPC 42.5R was determined using the laser particle size analyzer named LS-POP (9), which was shown in Fig. 1. Distilled water was used to mix the tailings and OPC 42.5R.

The chemical composition of the tailings and OPC 42.5R were tested using a sequential X-ray fluorescence spectrometer from the University of Science and Technology Beijing. In this section, the scanning speed, voltage, and current were 300°/min, 60 kV, and 140 mA, respectively. The chemical composition of the gold tailings and OPC 42.5R were shown in Fig. 2.

### 2.2 Basic Parameters of 3D-PP

The types of 3D printed polymer (3D-PP) materials used in this experiment were ordinary resin (OR) and thermoplastic polyurethanes (TPU). The basic physical and mechanical parameters of the 3D-PP materials were shown in Table 1. In addition, the types of 3D-PP were set in four types: cross, quarter, six equal parts (SEP), and eight equal parts (EEP). The model was constructed using Rhino3D modeling software and saved as a.STP and .STL file. The model was printed using a 3D printer from Beijing Hengyue Hongda Technology Co., Ltd, shown in Fig. 3. The height and diameter of the 3D-PP were 97 mm and 48 mm, respectively, taking into account the subsequent demoulding of the specimens. It is slightly smaller than a standard cylindrical mould (height and diameter 100 mm and 50 mm, respectively).

### 2.3 Specimens Preparation and Curing Conditions

This experiment's solid content and curing time were 70 wt% and 7d, respectively. In general, the cement-to-tailings ratio was between 1:4 and 1:10 in the cut and fill mining method (Cao et al. 2019). Thus, the cement-to-tailings ratio of 1:4, 1:6, 1:8, and 1:10 were used as control groups for the ordinary CTB specimens. The cement-to-tailings ratio of the 3D-PP reinforced CTB specimens was 1:10. The tailings, OPC 42.5R, and distilled water were weighed using
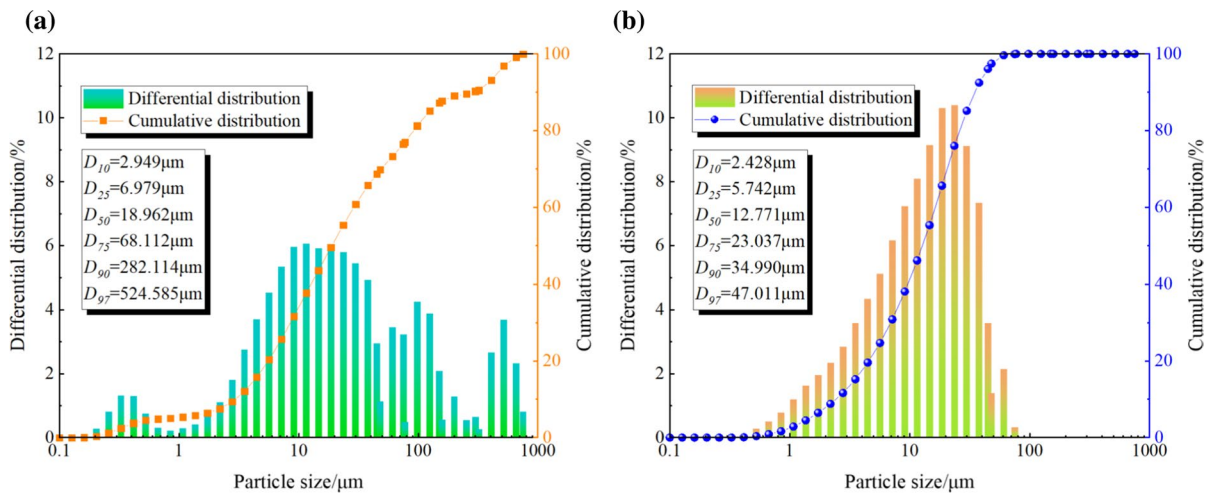
**(a)**



**(b)**



**Fig. 1** The particle size distribution of tailings and 42.5R cement
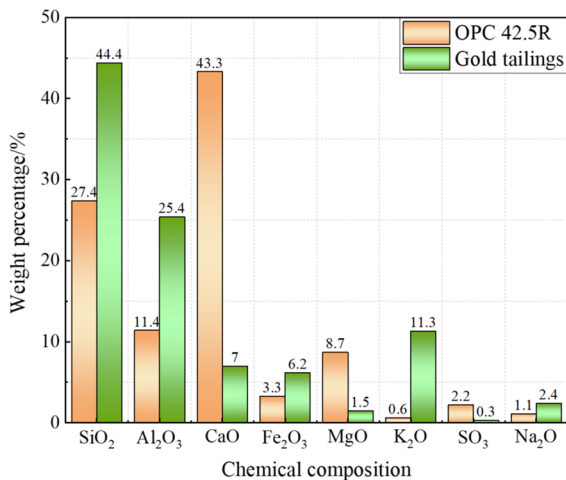


**Fig. 2** Chemical composition of FGT and OPC 42.5R

**Table 1** Basic parameters of polymer materials used in this test

| Polymer material | Compression strength (MPa) | Elastic modulus (MPa) | Water absorption (%) | Density (g/cm$^3$) | Fracture ductility |
|---|---|---|---|---|---|
| OR | 67 | 2650 | 0.4 | 1.2 | 6–9% |
| TPU | 40 | / | 0.5 | 1.2 | 3.0% |

a standard electronic scale (accuracy 0.01 g), model YHC60001. The tailings, OPC 42.5R, and distilled water were mixed in a cement slurry mixer type JJ-5 for not less than 3 min, which was referenced Huang et al. (2021a). The 3D-PP skeletons were placed in a standard cylindrical mould. Then the prepared CTB slurry was poured into the mould. Huang et al. (2021a) has investigated the UCS of solid wastes (SWs) as a potential resource for backfilling under the Unconfined compression test. The chosen height and diameter were 100 mm and 50 mm, respectively. Finally, the CTB specimens were cured at a constant temperature (20±1℃) and humidity (90±5%) curing container named HSBY-40B. After 48 h, the specimens were demolished from the mold and then returned to the curing box until 7d (Huang et al. 2021a). The 3D-PP reinforced CTB specimens preparation process was shown in Fig. 4.

### 2.4 Unconfined Compression Tests

After curing 7d, both ends of the tested CTB specimens' sections were polished to ensure flatness. Moreover, the flatness of both ends of the specimens were controlled to within ± 0.02 mm. The wdwi-100 uniaxial compression test system from the Materials Testing Center of the University of Science and Technology Beijing was used for this test (shown in Fig. 5). The loading rate was set to 1 mm/min. The test data were recorded and stored in the computer during the entire loading process. To reduce test errors, three specimens were selected for each group. Furthermore, the average of UCS was obtained.

**Fig. 3** Models and Figures of 3D-PP in this study. **a** Cross, **b** Quarter, **c** SEP and **d** EEP
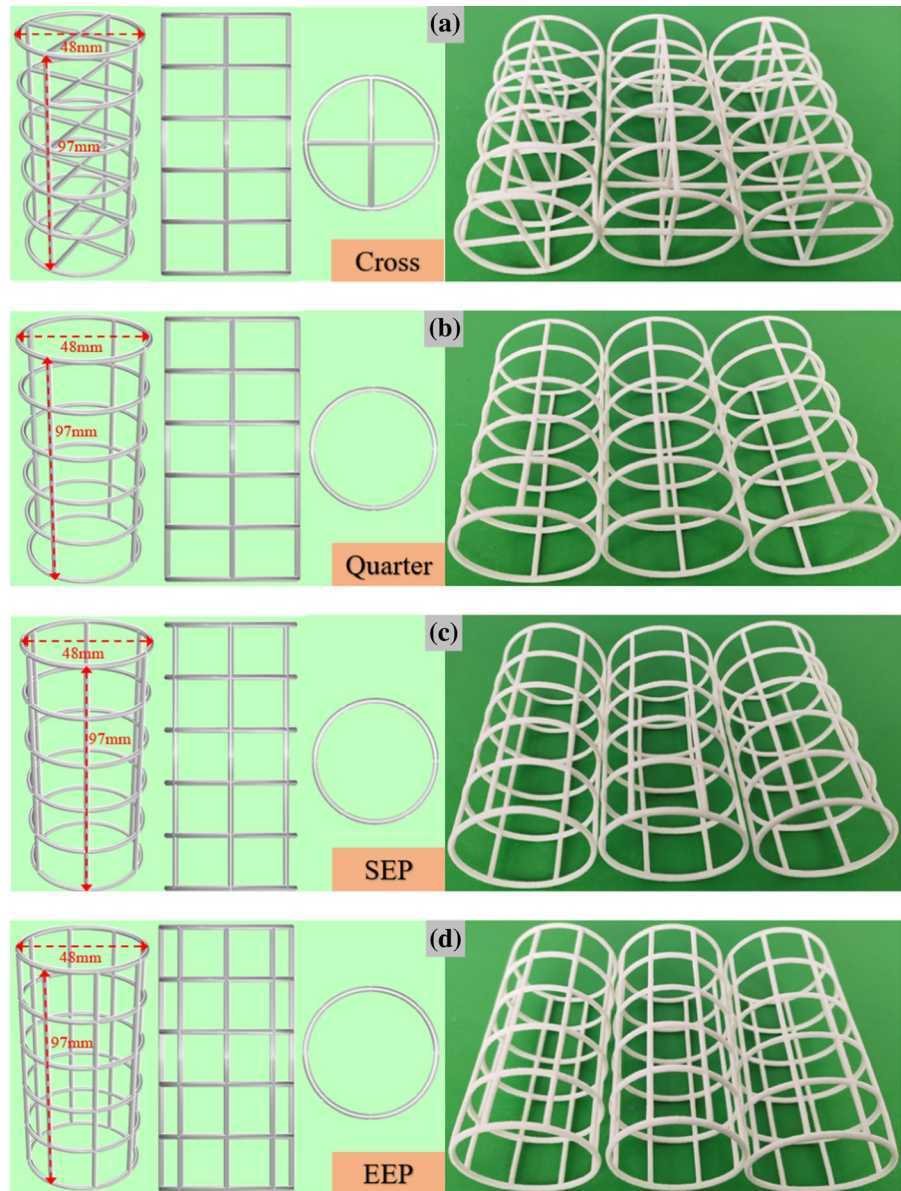


### 2.5 Scanning Electron Microscopy (SEM) Test

The morphology of hydration products and the distribution of microcracks in the specimens were analyzed using a Zeiss Evo 18 scanning electron microscope test system (SEM) at the Materials Testing Centre of the University of Science and Technology Beijing. The basic parameters of the microscope used were: the accelerating voltage was between 10 and 20 kV; the maximum magnification and resolution were 2000 times and 3 nm, respectively. Before the experiment, the observed samples must be dried, and then CTB samples were sprayed with diamond by vacuum coating. The CTB samples should be placed in the vacuum chamber for at least 20 min before scanning. The SEM observation process was shown in Fig. 6.
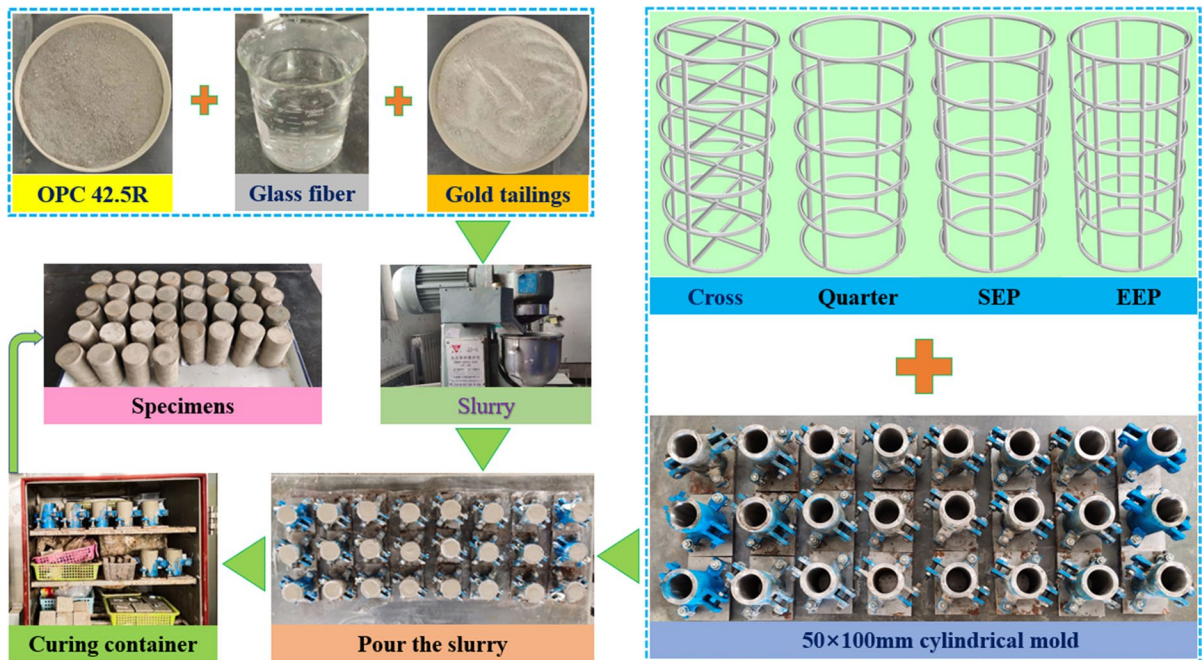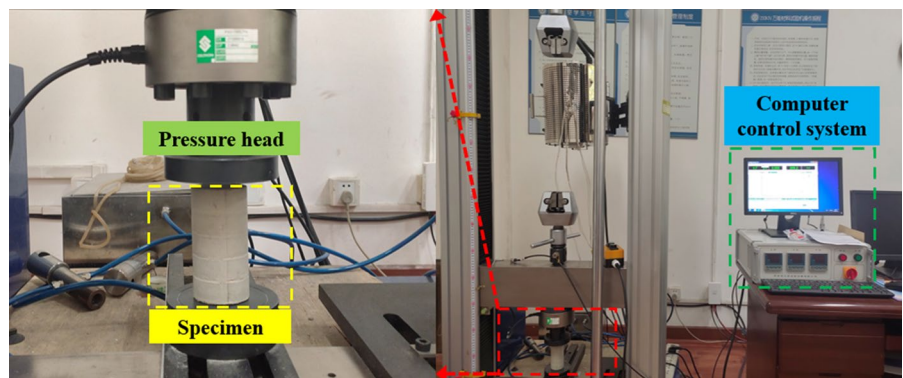
**Fig. 4** Preparation process of test specimens

**Fig. 5** Uniaxial compressive testing system



## 3 Results and Discussion

### 3.1 Effect of 3D-PP on the UCS

The UCS growth rate was defined to investigate the mechanism effect of the 3D-PP skeleton on the CTB's UCS, as shown in equation (1) (Qin et al. 2021).

$$f = \frac{f_{3D-PP} - f_{N-3D-PP}}{f_{N-3D-PP}} \times 100\% \tag{1}$$

where $f$ was the growth rate of UCS; $f_{3D-PP}$ was the UCS of 3D-PP reinforced-CTB; $f_{N-3D-PP}$ was the UCS of ordinary CTB (KB-1:8, KB-1:10).

The relationship between the UCS of the CTB and the different types of 3D-PP was shown in Fig. 7. Take the specimen numbered 'KB-1:8' as an example, where 'KB' was no 3D-PP added, and '1:8' was the cement-to-tailings ratio of the CTB. Take the specimen numbered 'OR- Cross' was an example, where 'OR' was ordinary resin, and 'Cross' was the 3D-PP skeleton shape. From Fig. 7b, it can be seen that the average UCS of the ordinary CTB were
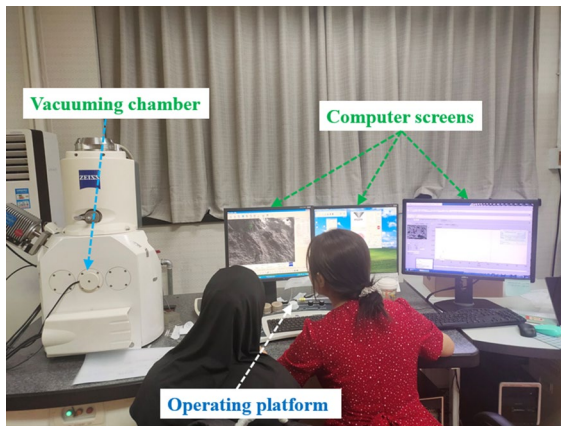
**Fig. 6** The ZEISS EVO 18 SEM testing system

2.54 MPa, 1.12 MPa, 0.71 MPa, and 0.59 MPa when the cement-to-tailings ratio were 1:4, 1:6, 1:8, and 1:10, respectively. Moreover, as can be seen from Fig. 7a, when the cement-to-tailings ratio was 1:10, the average UCS of the added OR-Cross, OR-Quarter, OR-SEP, and OR-EEP specimens were 0.80 MPa, 0.74 MPa, 0.70 MPa, and 0.72 MPa, respectively. The average UCS of the TPU-Cross, TPU-Quarter, TPU-SEP and TPU-EEP specimens were 0.47 MPa, 0.42 MPa, 0.39 MPa, and 0.43 MPa, respectively. The above results showed that OR-3D-PP could significantly increase the UCS of the CTB. However, instead of enhancing the UCS of the CTB, the TPU-3D-PP reduced it. The reason for this may be the low strength of the TPU itself, which was prone to pulling off and breaking underloading.

In addition, the UCS of the OR-3D-PP reinforced CTB were significantly improved, as can be seen in Fig. 7c. Compared with ordinary CTB with the cement-to-tailings ratio of 1:10, the UCS growth rates were 36.6%, 20.3%, 18.6%, and 22%, respectively. In contrast, the UCS growth rates of TPU-3D-PP reinforced CTB were − 20%, − 28.8%, − 33.9% and − 27.1%. From Fig. 7d, it can be found that the UCS growth rates of the OR-3D-PP reinforced CTB were 12.7%, 4.2%, − 1.4%, and 1.4%, respectively, compared to the ordinary CTB with the cement-to-tailings ratio of 1:8. The UCS growth rates for TPU-3D-PP reinforced CTB were − 33.8%, − 40.8%, − 45.1% and − 39.4%, respectively. The above results showed that OR-Cross-3D-PP had the best reinforcing effect on the UCS of the CTB. However, TPU-SEP-3D-PP

had a weakening effect on the UCS of the CTB, which had the lowest UCS.

## 3.2 Effect of 3D-PP on Stress–Strain Relation

Figure 8 showed the stress–strain relationship curve of the ordinary CTB, and the 3D-PP reinforced CTB.

As shown from Fig. 8, the stress–strain curves of the ordinary CTB and the 3D-PP reinforced CTB could be roughly divided into the pore compaction stage, the linear elastic stage, and the unstable rupture, and the crack propagation stage. After the specimens had reached their peak compressive strength, as the load continued to be applied, the cracking of the specimens continued to expand until the specimens were destroyed. However, the stress–strain curves of the OR-3D-PP reinforced CTB specimens were mainly similar to the other specimens in the pore compaction and linear elastic stage. The stress–strain curves of the specimens in the latter two stages were significantly different. The curve showed a rise, then a fall, then a continued rise, and finally a sudden fall. The main cause may be that the CTB block on the surface of the specimens falls off during the loading process. As the load continued to be applied, the 3D-PP support became more pronounced due to the toughness of the OR. When the 3D-PP reached its breaking strength, the curve showed a sudden drop.

## 3.3 Effect of 3D-PP on Toughness Properties of CTB Specimens

For 3D-PP reinforced CTB, toughness was considered a more appropriate way to characterize the properties of 3D-PP than single parameters such as compressive strength, flexural strength, or modulus of rupture. The peak strain factor 'K' was defined as a toughness evaluation parameter to investigate the effect of 3D-PP on the toughness of the CTB. It was shown in equation (2) (Cao et al. 2019).

$$K = \frac{\varepsilon_{\mathrm{f}}}{\varepsilon_{\mathrm{n}}} \tag{2}$$

where $\varepsilon_{\mathrm{f}}$ was the peak strain of the 3D-PP reinforced CTB; $\varepsilon_{\mathrm{n}}$ was the peak strain of the KB-1:10 CTB.

Figure 9 showed the parameters for evaluating the toughness of the 3D-PP reinforced CTB.
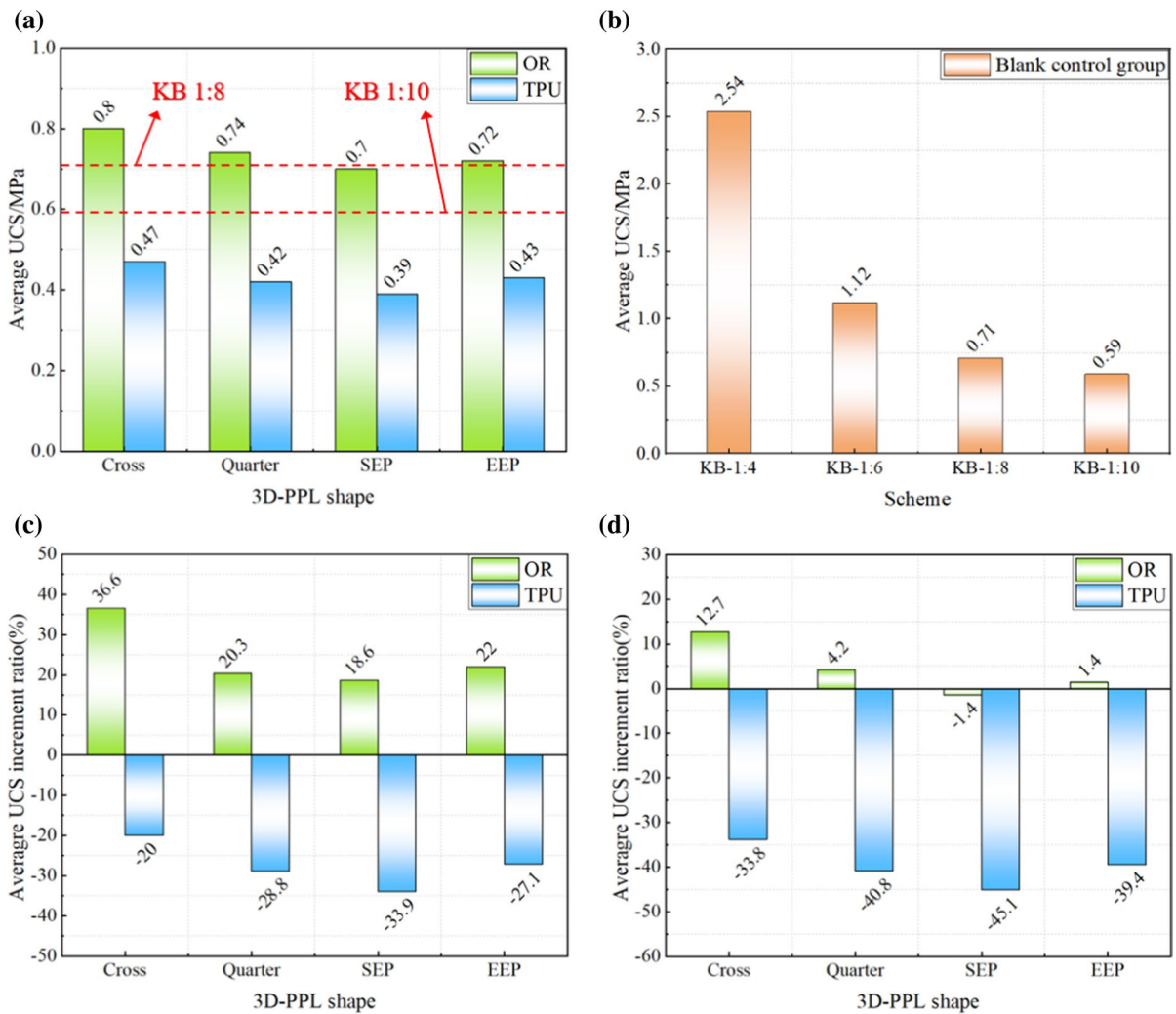
**Fig. 7** Bar charts between average UCS and 3D-PP shape: **a** Add 3D-PP average UCS; **b** Blank control group average UCS; **c** Average UCS increment ratio (KB-1:10); **d** Average UCS increment ratio (KB-1:8)

As shown in Fig. 9, the 'K' values for the OR-3D-PP reinforced CTB specimens were 16.7, 15.1, 10.3, and 7.3, respectively. Of these, the OR-Cross-3D-PP reinforced CTB had the best toughness. However, the 'K' values for the TPU-3D-PP reinforced CTB specimens were 1.1, 0.96, 1.4, and 1.5, respectively. As can be seen from the comparison, the OR-3D-PP can significantly enhance the toughness of the CTB. In contrast, TPU-3D-PP had a negligible effect on the toughness of the CTB or even a weakening effect. In addition, the most significant toughness-enhancing effect on the CTB were seen with the OR-Cross-3D-PP. It was due to the better mechanical properties of the OR.
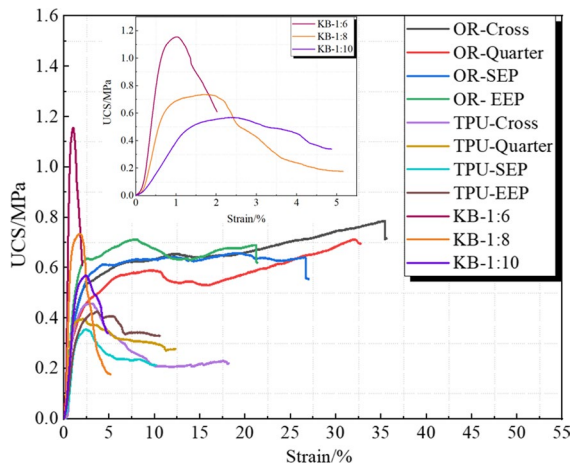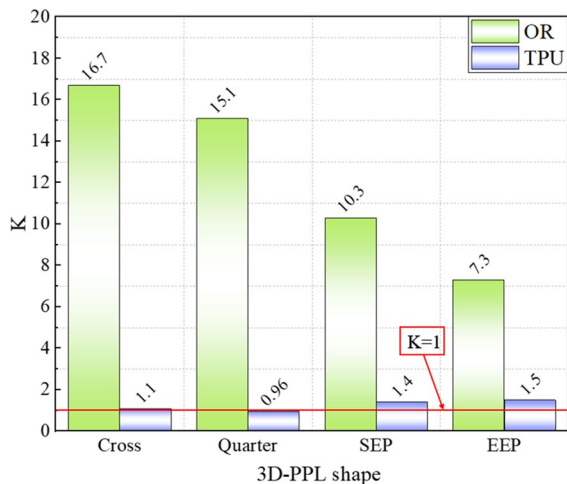
**Fig. 8** Stress–strain curve of the CTB specimens



**Fig. 9** Toughness evaluation parameter of 3D-PP reinforced CTB

### 3.4 Effect of 3D-PP on the Failure Evolution of CTB Specimens

Figure 10 showed the stress–strain curves and failure evolution process of the 11 types of CTB specimens. As can be seen from the figure, the 3D-PP reinforced CTB specimens' failure evolution process was slower than the ordinary CTB specimens. In addition, OR-3D-PP reinforced CTB had the highest level of final damage. It indicated that it could absorb more energy during the loading process. It corresponded to the stress–strain curve in Fig. 8. It was also found that the cracks appeared first in the middle of the specimens during the loading process. The cracks gradually extended upwards and downwards until the specimens were finally damaged. However, the form of damage in TPU-3D-PP reinforced CTB were different. The cracks first appeared in the middle of the specimens. However, the cracks gradually expanded upwards until the specimens were finally damaged. The failure mode of the ordinary CTB specimens were mainly tensile damage.

### 3.5 Microstructural analysis

Figure 11 showed the microstructure of the ordinary CTB, and the 3D-PP reinforced CTB. As shown from Fig. 11d, all the CTB specimens produced large amounts of hydration products such as ettringite (AFt) and C–S–H gels internally. In addition, Fig. 11a showed that in the 3D-PP reinforced CTB specimens, the traces of hydration products in contact with the 3D-PP were relatively clear. It indicated that the hydration products of the 3D-PP reinforced CTB specimens detach from the 3D-PP under load. At the same time, many microcracks were produced on the surface of the CTB specimens. The Image J software was used to measure the trace widths. First, the photo was imported into the related software, and the trace widths could be calibrated using the size and pixel conversion function. The traces widths in the contact zone of the 3D-PP skeleton and hydration products were 761.1 μm, 738.3 μm, 853.2 μm, and 737.9 μm respectively. The uneven loading of different parts of the 3D-PP skeleton may result in different degrees of skeleton deformation during the loading process. It eventually led to the separation of the skeleton from the hydration products.

Meanwhile, it can be seen from Fig. 11b, c that there were many micro-cracks on the surface of the OR-3D-PP reinforced CTB specimens. It indicated that the CTB specimens absorbed energy through the deformation of the 3D-PP skeleton under external loading. The crack expansion also absorbed more energy. It resulted in a higher UCS of the CTB specimens.

**Fig. 10** Failure evolution of CTB specimens: **a** OR-Cross; **b** OR-Quarter; **c** OR-SEP; **d** OR-EEP; **e** TPU-Cross; **f** TPU-Quarter; **g** TPU-SEP; **h** TPU-EEP; **i** KB-1:6; **j** KB -1:8; **k** KB-1:10
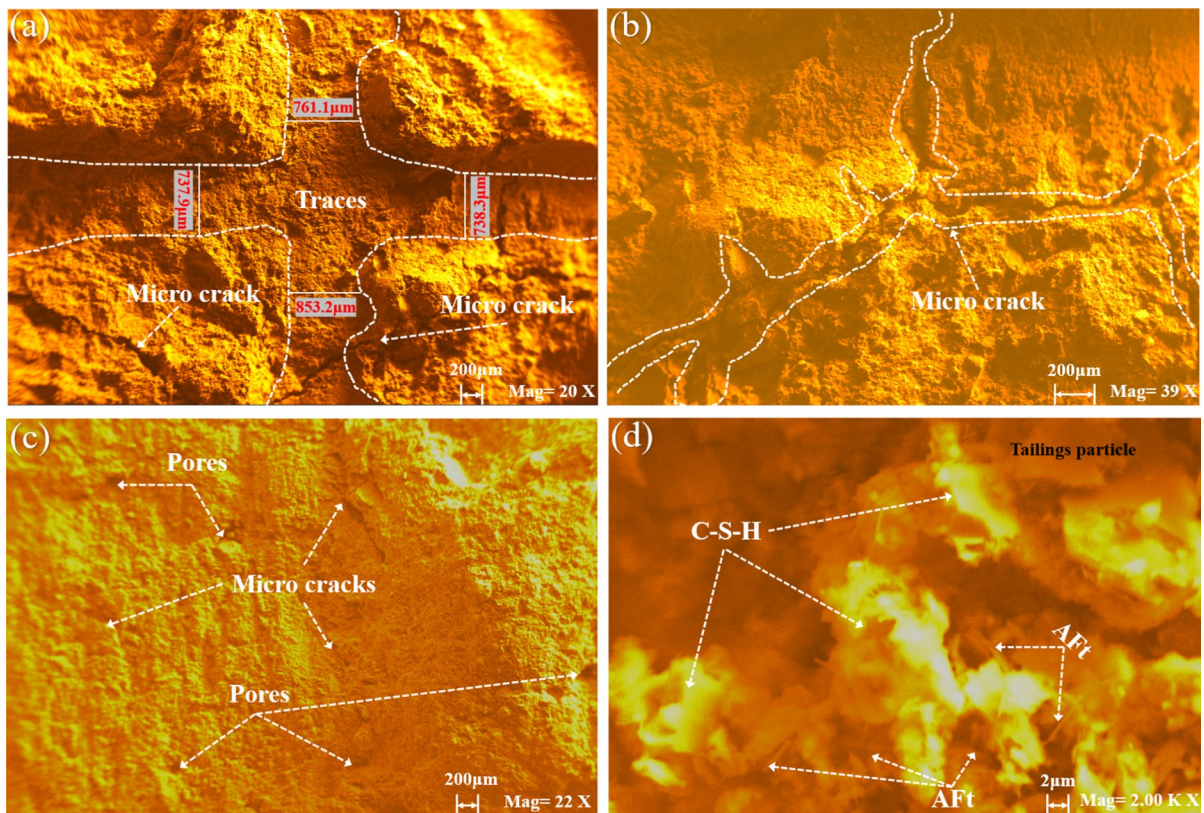
**Fig. 11** SEM images of the tested CTB specimens

## 4 Conclusion

This experiment carried out uniaxial compression tests, theoretical analysis, and scanning electron microscopy tests of the 3D-PP reinforced CTB, which investigated its macroscopic and macroscopic mechanical properties. The main conclusions are as follows:

(1) When the cement-to-tailings ratio was 1:10, the average UCS of the OR-Cross-3D-PP reinforced CTB was 0.8 MPa. Compared with ordinary CTB with the cement-to-tailings ratio of 1:10 and 1:8, the growth rates of UCS were 36.6% and 12.7%, respectively. OR-Cross-3D-PP had an obvious strength enhancement effect.

(2) The 'K' values for the OR-3D-PP reinforced CTB specimens were 16.7, 15.1, 10.3, and 7.3, respectively. The OR-3D-PP can significantly enhance the toughness of the CTB.

(3) The 'K' values for the TPU-3D-PP reinforced CTB specimens were 1.1, 0.96, 1.4, and 1.5, respectively. TPU-3D-PP had a negligible effect on the toughness of the CTB or even a weakening effect.

(4) All the CTB specimens produced large amounts of hydration products such as ettringite (AFt) and C–S–H gels internally. The uneven loading of different parts of the 3D-PP skeleton during the loading process, resulting in different degrees of skeleton deformation. It eventually led to the separation of the skeleton from the hydration products.

In this article, the author had carried out a preliminary exploration of the macroscopic and microscopic mechanical properties of the 3D-PP reinforced CTB. In the future, the author will conduct in-depth research on the mechanism of 3D-PP and numerical simulation. It is expected to provide a

specific reference basis for the mechanical strength enhancement methods of the CTB in the future.

**Data Availability** Enquiries about data availability should be directed to the authors.

## Declarations

**Conflict of interest** The authors declare that the work described has not been published before, that it is not under consideration for publication anywhere else, that its publication has been approved by all co-authors, that there is no conflict of interest regarding the publication of this article.

## References

Cao S, Yilmaz E, Song WD (2019) Fiber type effect on strength, toughness and microstructure of early age cemented tailings backfill. Constr Build Mater 223:44–54. https://doi.org/10.1016/j.conbuildmat.2019.06.221

Cao S, Yilmaz E, Yin ZY, Xue GL (2020) Assessment of rheological and sedimentation characteristics of fresh cemented tailings backfill slurry. Int J Min Reclam Environ 10:319–335. https://doi.org/10.1080/17480930.2020.1826092

Chen X, Shi X, Zhou J et al (2020) Determination of mechanical, flowability, and microstructural properties of cemented tailings backfill containing rice straw. Constr Build Mater 246:118520. https://doi.org/10.1016/j.conbuildmat.2020.118520

Cheng AP, Zhang YS, Dai SY, Dong FS, Zeng WX, Li DF (2019) Space-time evolution of acoustic emission parameters of cemented backfill and its fracture prediction under uniaxial compression. Rock Soil Mech 40(8):2965–2974. https://doi.org/10.16285/j.rsm.2018.1940

Ding T, Xiao JZ, Zou S et al (2021) Flexural properties of 3D printed fibre-reinforced concrete with recycled sand. Constr Build Mater 288:123077. https://doi.org/10.1016/j.conbuildmat.2021.123077

Hamdaoui O, Limam O, Ibos L, Mazioud A (2021) Thermal and mechanical properties of hardened cement paste reinforced with Posidonia-oceanica natural fibers. Constr Build Mater 269:121339. https://doi.org/10.1016/j.conbuildmat.2020.121339

He Y, Zhang QL, Chen QS, Bian JW, Qi CC, Kang Q, Feng Y (2021) Mechanical and environmental characteristics of cemented paste backfill containing lithium slag-blended binder. Constr Build Mater 271:121567

Hou YQ, Yin SH, Yang SX, Zhang MZ, Liu HB (2021) Study on the mechanical response and energy damage evolution process of cemented backfill under impact loading. Rock Soil Mech 43(supp1):2965–2974

Huang ZQ, Yilmaz E, Cao S (2021a) Analysis of strength and microstructural characteristics of mine backfills containing fly ash and desulfurized gypsum. Minerals 11(4):409. https://doi.org/10.3390/min11040409

Huang ZQ, Cao S, Yilmaz E (2021b) Investigation on the flexural strength, failure pattern and microstructural characteristics of combined fibers reinforced cemented tailings backfill. Constr Build Mater 300:124005. https://doi.org/10.1016/j.conbuildmat.2021.124005

Li JJ, Yilmaz E, Cao S (2021) Influence of industrial solid waste as filling material on mechanical and microstructural characteristics of cementitious backfills. Constr Build Mater 299(13):124288. https://doi.org/10.1016/j.conbuildmat.2021.124288

Liu L, Xin J, Huan C et al (2020b) Effect of curing time on the mesoscopic parameters of cemented paste backfill simulated using the particle flow code technique. Int J Miner Metall Mater 28(4):590–602. https://doi.org/10.1007/s12613-020-2007-2

Liu HF, Zhang JX, Li BY et al (2021) Long term leaching behavior of arsenic from cemented paste backfill made of construction and demolition waste: experimental and numerical simulation studies. J Hazard Mater 416:125813. https://doi.org/10.1016/j.jhazmat.2021.125813

Liu L, Xin J, Qi CC et al (2020a) Experimental investigation of mechanical, hydration, microstructure and electrical properties of cemented paste backfill. Constr Build Mater. https://doi.org/10.1016/j.conbuildmat.2020.120137

Min CD, Li XB, He SY, Zhou ST, Zhou YN, Shan Yang S, Ying Shi Y (2019) Effect of mixing time on the properties of phosphogypsum-based cemented backfill. Constr Build Mater 210:564–573. https://doi.org/10.1016/j.conbuildmat.2019.03.187

Qin SW, Cao S, Yilmaz E, Li JJ (2021) Influence of types and shapes of 3D printed polymeric lattice on ductility performance of cementitious backfill composites. Constr Build Mater 307:124973. https://doi.org/10.1016/j.conbuildmat.2021.124973

Wang S, Song XP, Chen QS, Wang XJ, Wei ML, Ke YX, Luo ZH (2020) Mechanical properties of cemented tailings backfill containing alkalized rice straw of various lengths. J Environ Manage 276:111124. https://doi.org/10.1016/j.jenvman.2020.111124

Wang YY, Yu ZQ, Wang HW (2021a) Experimental investigation on some performance of rubber fiber modified cemented paste backfill. Constr Build Mater 271:121586. https://doi.org/10.1016/j.conbuildmat.2020.121586

Wang YY, Yu ZQ, Wang HW (2021b) Experimental investigation on some performance of rubber fiber modified cemented paste backfill. Constr Build Mater 271:121586. https://doi.org/10.1016/j.conbuildmat.2020.121586

Xu XD, Sun GH, Yao XL, Yao XL, Liang XJ, Shao LH (2021) A cusp catastrophe waring model for instability of backfill based on energy dissipation and release. Rock Soil Mech 41(9):3003–3012

Xu WB, Li QL, Tian MM (2019) Strength and deformation properties of polypropylene fiber-reinforced cemented tailings backfill. Chin J Eng 41(12):1618–1626. https://doi.org/10.13374/j.issn2095-9389.2018.12.14.002

Xue GL, Yilmaz E, Song WD, Cao S (2020) Fiber length effect on strength properties of polypropylene fiber reinforced

cemented tailings backfill specimens with different sizes. Constr Build Mater 241:118113. https://doi.org/10.1016/j.conbuildmat.2020.118113

Xue GL, Yilmaz E, Feng GR, Cao S (2021) Bending behavior and failure mode of cemented tailings backfill composites incorporating different fibers for sustainable construction. Constr Build Mater 289:123163. https://doi.org/10.1016/j.conbuildmat.2021.123163

Zhao K, Huang M, Yan YJ, Wan WL, Ning FJ, Zhou Y, He ZW (2021) Study on mechanical properties and cooperative deformation of tailings cemented filling material assembly with different lime-sand ratios. Chin J Rock Mech Eng 40(S1):2781–2789

Zheng D, Song WD, Fu JX et al (2020a) Research on mechanical characteristics, fractal dimension and internal structure of fiber reinforced concrete under uniaxial compression. Constr Build Mater. https://doi.org/10.1016/j.conbuildmat.2020.120351

Zheng D, Song WD, Tan YY et al (2020b) Research on fractal and microscopic quantitative characterization of unclassified tailings flocs. Int J Miner Metall Mater. https://doi.org/10.1007/s12613-020-2181-2

Zheng D, Song WD, Tan YY, Cao S, Yang ZL (2021) Fractal and microscopic quantitative characterization of unclassified tailings flocs. Int J Miner Metall Mater 28(9):1429–1439. https://doi.org/10.1007/s12613-020-2181-2